PCO: Precision-Controllable Offset Surfaces with Sharp Features - Supplementary Material

LEI WANG, Shandong University, China
XUDONG WANG, Shandong University, China
PENGFEI WANG, Shandong University, China
SHUANGMIN CHEN*, Qingdao University of Science and Technology, China
SHIQING XIN, Shandong University, China
JIONG GUO, Shandong University, China
WENPING WANG, Texas A&M University, USA
CHANGHE TU, Shandong University, China

ACM Reference Format:
Lei Wang, Xudong Wang, Pengfei Wang, Shuangmin Chen, Shiqing Xin, Jiong Guo, Wenping Wang, and Changhe Tu. 2024. PCO: Precision-Controllable Offset Surfaces with Sharp Features - Supplementary Material . *ACM Trans. Graph.* 1, 1 (November 2024), 8 pages. https://doi.org/10.1145/3687920

A PROOF OF THEOREM 4.1

For any pair of points $\{p_1, p_2\}$ within the circumsphere of a tetrahedron T, their straight-line distance $d(p_1, p_2)$ must satisfy

$$d(p_1, p_2) \leq 2R, \tag{1}$$

where R is the radius of the circumsphere. Therefore, if

$$\max_{k=1}^{4}\{d^{(k)}(\mathcal{M}; T)\} > \delta + 2R \tag{2}$$

or

$$\min_{k=1}^{4}\{d^{(k)}(\mathcal{M}; T)\} < \delta - 2R, \tag{3}$$

then T cannot contribute to the offset at δ. Fig. 1 (a) and (b) illustrate two 2D examples for these scenarios respectively.

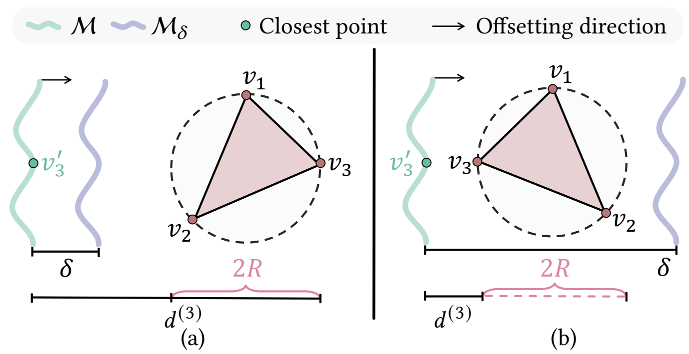

Fig. 1. In this 2D example, the triangle represents a 3D tetrahedron, while the base surface $\mathcal{M}$ and the offset surface $\mathcal{M}_\delta$ are depicted as green and purple curves, respectively. We abbreviate $d^{(k)}(\mathcal{M}; T)$ as $d^{(k)}$ for simplicity. In (a), the maximum vertex distance, $d^{(3)}$, exceeds $\delta + 2R$, indicating that the triangle does not contribute to the offset at δ. In (b), the minimum vertex distance, $d^{(3)}$, is less than $\delta - 2R$, showing that the triangle also does not contribute to the offset at δ.

B ANALYSIS OF THE MERGED FIELD FORM

Considering the scenario where $\delta > 0$ (with an analogous case for $\delta < 0$). Let the merged field of $\mathbf{D}_1$ and $\mathbf{D}_2$ be denoted as $\mathbf{D}_{12}$. Define P and E as the sets of intersection points and edges of the tetrahedron T in $\{T \cap \pi_1^+ \cap \pi_2^+\}$, where π_u defined by $\mathbf{D}_u = \delta$.

If $E = \emptyset$, any $p \in P$ must coincide with a vertex v_k of T ($k = 1, 2, 3, 4$), implying $\mathbf{D}_1(k) = \mathbf{D}_2(k) = \delta$. Therefore, $p \in \pi_{12}^=$.

If $E \neq \emptyset$, let $p \in P$ be the intersection of an edge $e = (v_i, v_j) \in E$ with $1 \leq i, j \leq 4$. Then π_{12} must intersect with e, and we can deduce that $f = f_i \cdot f_j = (\mathbf{D}_{12}(i) - \delta) \cdot (\mathbf{D}_{12}(j) - \delta) \leq 0$.

(1) If $f = 0$:
- $f_i = 0$ and $f_j = 0$: $\mathbf{D}_{12}(i) = \mathbf{D}_{12}(j) = \delta$, any p on e satisfies $p \in \pi_{12}^=$,
- $f_i = 0$ and $f_j \neq 0$: p coincides with v_i, hence $p \in \pi_{12}^=$,
- $f_j = 0$ and $f_i \neq 0$: p coincides with v_j, hence $p \in \pi_{12}^=$.

(2) If $f < 0$:
Consider the function $h(x, y; \delta)$:

$$\begin{cases} \frac{\delta - x}{y - x} & (-\infty, \delta] \times [\delta, +\infty) \setminus (\delta, \delta) \\ 0 & (x, y) = (\delta, \delta) \end{cases} \tag{4}$$

---

*Corresponding author: Shuangmin Chen.

Authors' addresses: Lei Wang, Shandong University, Qingdao, Shandong, China, leiw1006@gmail.com; Xudong Wang, Shandong University, Qingdao, Shandong, China, sduwxd0319@gmail.com; Pengfei Wang, Shandong University, Qingdao, Shandong, China, pengfei1998@foxmail.com; Shuangmin Chen, Qingdao University of Science and Technology, Qingdao, Shandong, China, csmqq@163.com; Shiqing Xin, Shandong University, Qingdao, Shandong, China, xinshiqing@sdu.edu.cn; Jiong Guo, Shandong University, Qingdao, Shandong, China, xhjia@amss.ac.cn; Wenping Wang, Texas A&M University, Texas, USA, wenping@tamu.edu; Changhe Tu, Shandong University, Qingdao, Shandong, China, chtu@sdu.edu.cn.

0730-0301/2024/11-ART $15.00
https://doi.org/10.1145/3687920

The partial derivatives of h with respect to x and y are $h_x < 0$ and $h_y < 0$ respectively for $x \in (-\infty, \delta), y \in (\delta, +\infty)$. Suppose p^* is the intersection of π_{12} on e, its position can be calculated as

$$p^* = v_i + h(\mathbf{D}_{12}(j), \mathbf{D}_{12}(i); \delta)(v_j - v_i). \tag{5}$$

Given that $\mathbf{D}_{12} = \mathbf{S} \odot \min(|\mathbf{D}_1|, |\mathbf{D}_2|)$, if $\mathbf{S} > 0$, point p must lie below the intersection p^*.

In conclusion, the half-plane π_{12} defined by $\mathbf{D}_{12} = \delta$ satisfies

$$\begin{aligned} &\{T \cap \pi_{12}^{+}\} \subset \{T_i \cap \pi_1^{+=} \cap \pi_2^{+=}\} && \text{if } \delta > 0 \text{ and } \mathbf{S} > 0, \\ &\{T \cap \pi_{12}^{-}\} \subset \{T_i \cap \pi_1^{-=} \cap \pi_2^{-=}\} && \text{if } \delta < 0 \text{ and } \mathbf{S} < 0. \end{aligned} \tag{6}$$

C IMPLEMENTATION DETAILS

Distance Calculator. Our algorithm supports both signed and unsigned distance computations.

For the direct computation of signed distances, the main challenge lies in determining the sign of a point p (e.g., a vertex of a tetrahedron). In our implementation, we employed several methods for this purpose, including pseudo-normals [Bærentzen and Aanaes 2005], ray intersection [Cherchi et al. 2022], and winding number [Barill et al. 2018; Jacobson et al. 2013]. Each method presents a trade-off between robustness and efficiency. However, these approaches struggle with imperfect meshes, such as non-manifold, or non-watertight meshes, due to undefined orientations. In such cases, we recommend using unsigned distance computations, which yield two offset results meanwhile—inward and outward. Since our results retain excellent properties of being watertight, manifold, and free of self-intersections, we can accurately extract the internal and external results using straightforward sign determination methods.

Analysis of Half-plane Cutting Process. Our incremental half-plane cutting process can become time-consuming if all contributing triangles are included in the distance field computation within a tetrahedron. To mitigate this, we implement an effective triangle filtering process.

Before delving into details, we first define the "competitive relationship" between two linear distance fields $\mathbf{D}_1$ and $\mathbf{D}_2$ within a tetrahedron T.

Definition C.1. The distance field $\mathbf{D}_1$ is defeated by $\mathbf{D}_2$ only when $\{\pi_1^+ \cap T\} \cap \{\pi_2^+ \cap T\} = \{\pi_2^+ \cap T\}$, where π_i^+ is the positive side of half-plane π_i defined by $\pi_i = \delta$, $i = 1, 2$.

If one distance field is defeated by another, it is not considered valid for participation in the half-plane cutting process. Based on this definition, we propose the following theorem:

Theorem C.2. *If the distance field* $\mathbf{D}_1$ *is defeated by* $\mathbf{D}_2$*, it must satisfies* $\min |\mathbf{D}_1| > \max |\mathbf{D}_2|$.

Further, let C_t^T denote the contributing triangles of T:

$$C_t^T = \{t | t \text{ has the contribution to } T\}.$$

According to the above theorem C.2, we can deduce the following lemma:

Lemma C.3. *Let* Prj_{t_i} *be the projected triangle on the original mesh of vertex* $v_i (i = 1, 2, 3, 4)$ *in* T*, where* $\text{Prj}_{t_i} \in C_t^T$*. The triangle is impossible defeated by other triangles in* C_t^T*.*

The proof is straightforward: the field $|\mathbf{D}_{\text{Prj}_{t_i}}|$ at least has one minimum value compared with other distance fields whose source triangles are belong to C_t^T.

Following the above theories, we first compute the distance fields $\mathbf{D}_{\text{Prj}_{t_i}}$ from the triangles Prj_{t_i}. Subsequently, we maintain the maximum distance values of four vertexes in T using a quadruple $\mathbf{M}_T$, initialized as

$$\mathbf{M}_T(j) = \max_{i=1,2,3,4} \{\mathbf{D}_{\text{Prj}_{t_i}}(j)\}, j = 1, 2, 3, 4. \tag{7}$$

Only the newly distance field $|\mathbf{D}|$ satisfies

$$\max |D| < \min |\mathbf{M}_T|, \tag{8}$$

it can be considered as a valid one to involve in the subsequent half-plane cutting process.

D EXPERIMENTAL DETAILS AND RESULTS

D.1 Evaluation metrics

We use relative one-sided Chamfer distance (d_{C}), relative one-sided Hausdorff distance (d_{H}), Mean Absolute Normal deviation (N_{MAE}), and Normal Score (N-Score) to evaluate the accuracy of offsetting results. We denote $r = |\delta|$, $\mathcal{M}_\delta$ and $\mathcal{M}$ as the offsetting mesh at δ and the input mesh, respectively. Let P_1 and P_2 be the randomly sampled points from $\mathcal{M}_\delta$ and $\mathcal{M}$.

Distance error metrics. The relative one-sided ($P_1 \longrightarrow P_2$) Chamfer distance and Hausdorff distance between two point clouds P_1 and P_2 are defined as follows:

$$\begin{aligned} d_{\text{C}} &= \frac{1}{r * |P_1|} \sum_{p_1 \in P_1} |\min_{p_2 \in P_2} d(p_1, p_2) - \delta| \\ d_{\text{H}} &= \frac{1}{r} \max_{p_1 \in P_1} \min_{p_2 \in P_2} |d(p_1, p_2) - \delta|, \end{aligned} \tag{9}$$

where $d(p_1, p_2)$ is the straight-line distance between points p_1, p_2. We use the $L - 1$ norm following [Wang and Manocha 2013; Zint et al. 2023].

Normal consistency metrics. The metrics of Mean Absolute Error of normal deviation and Normal Score at a given threshold γ between two point clouds P_1 and P_2 are defined as follows:

$$\begin{aligned} \text{N}_{\text{MAE}} &= \frac{1}{|P_1|} \sum_{p_1 \in P_1} \text{angle}(\mathbf{n}_{p_1}, \mathbf{n}_{\text{closest}(p_1, P_2)}) \\ \text{N-Score} &= \frac{|\{\text{angle}(\mathbf{n}_p, \mathbf{n}_{\text{closest}(p_1, P_2)}) < \gamma\}|}{|P_1|}, \end{aligned} \tag{10}$$

where

$$\text{closest}(p, P) = \arg\min_{p' \in P}(p, p'), \tag{11}$$

and

$$\text{angel}(\mathbf{n}_p, \mathbf{n}'_p) = \arccos(\mathbf{n}_p \cdot \mathbf{n}'_p). \tag{12}$$

In our experiments, $\gamma = 5^{\circ}$.

D.2 Validation on Triangle Soup

Our algorithm exhibits impressive stability with respect to noisy triangle mesh - triangle soups, consistently ensuring valid output, as shown in Fig. 2.

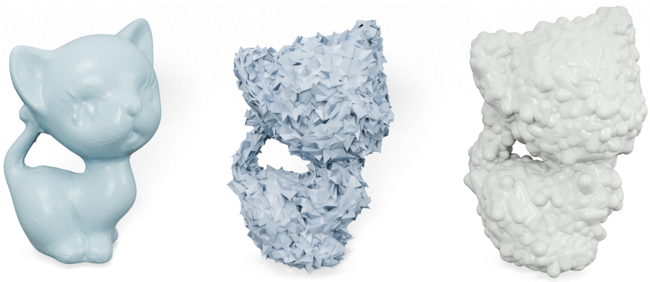

(a) Kitten (106 K) (b) Noisy soup (c) 2% offset

Fig. 2. Our method effectively processes triangle soups and ensures that the output is topology correct.

D.3 Integrated with Alpha Shape

When the complexity of and the input the offset distance are all very large, our algorithm may become time-consuming due to the large number of contributing triangles involved in distance field computation in each tetrahedron. However, leveraging our algorithm's effective sharp feature preservation, we offer an alternative approach to achieve efficiency without significantly sacrificing accuracy: initially employing alpha shape algorithm [Edelsbrunner and Mücke 1994] to compute a coarse result at a smaller offset distance, followed by applying our method.

As illustrated in Fig. 3, this decreases processing time by nearly 90% while still effectively maintaining the clarity of the feature lines.

Table 1. Quantitative comparison results on twisted and thin-plate models. The **best** scores are highlighted in bold with underlining, while the **second best** scores are highlighted in bold.

		94884		104559		213887	
		-0.5	1	-0.5	2	-0.5	0.5
Time/s	AW	-	365.96	-	204.38	-	203.45
	DC	257.84	268.63	142.77	146.02	207.07	211.78
	FPO	-	151.99	-	372.81	-	151.99
	HSP	**23.64**	**64.85**	**7.30**	**40.84**	**9.37**	**15.25**
	Ours	**5.08**	**8.64**	**1.86**	**11.67**	**2.22**	**4.25**
d_C ($\times10^{-3}$) ↓	AW	-	**0.780**	-	**0.553**	-	**2.152**
	DC	**1.214**	1.645	**5.845**	2.045	**1.188**	**4.180**
	FPO	-	9.040	-	8.448	-	19.851
	HSP	**10.833**	5.441	28.595	17.734	18.501	24.247
	Ours	20.299	**0.138**	**2.593**	**0.523**	**13.508**	31.296
d_H ($\times10^{-3}$) ↓	AW	-	**38.080**	-	38.756	-	**153.300**
	DC	**61.040**	46.821	**127.980**	**30.758**	**45.040**	**133.030**
	FPO	-	353.290	-	85.453	-	418.840
	HSP	399.820	170.280	795.140	1953.400	733.940	163.360
	Ours	**149.560**	**38.112**	**8.293**	**38.200**	**162.700**	206.760
N_{MAE} ↓	AW	-	**12.341**	-	28.424	-	16.982
	DC	**2.958**	12.565	**9.561**	30.731	**2.287**	15.892
	FPO	-	32.765	-	30.451	-	35.235
	HSP	8.464	12.499	24.663	**30.620**	7.712	**15.343**
	Ours	**4.978**	**2.358**	**7.172**	**1.732**	**3.314**	**4.159**
N-Score/% ↑	AW	-	74.00	-	32.30	-	65.39
	DC	**93.28**	**74.80**	**73.13**	**34.30**	**92.34**	**68.12**
	FPO	-	54.91	-	30.40	-	59.76
	HSP	**81.77**	73.00	2.80	28.70	62.55	64.20
	Ours	64.67	**82.15**	**44.82**	**97.05**	**76.61**	**71.48**

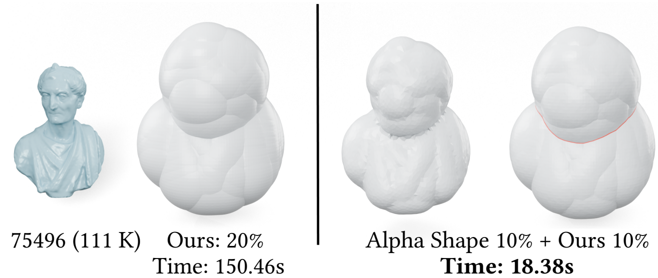

Fig. 3. To effectively manage time and ensure accurate results when dealing with complex models and significant offset distances, our method can be integrated with Alpha Shape [Edelsbrunner and Mücke 1994]. In this scenario, features are still accurately recovered with minimal time expenditure.

D.4 Comparison on CAD Models

We give the comparison statistics in Table 2. The corresponding visual comparison is given in Fig. 4, Fig. 5, and Fig. 6. It can be seen that our method achieves effectively balances accuracy and robustness, outperforming alternative methods in preserving fine features while maintaining overall structural integrity.

D.5 Comparison on Twisted and Thin-plate Models

The quantitative comparison statistics are reported in Table 1, while the visual comparison is available in Fig. 7. The comparison shows that our method is better at recovering thin geometry features and can achieve a good trade-off between smoothness and feature preservation.

D.6 Comparison on Models Reconstructed from Large Raw Scan Data

We show the visual comparison of different approaches with varying offset distance in Fig. 8, and the qualitative results are shown in Table 3. Both qualitative and quantitative comparisons show that our method can faithfully recover fine geometric details and thin structures, outperforming the other methods.

REFERENCES

Jakob Andreas Bærentzen and Henrik Aanaes. 2005. Signed distance computation using the angle weighted pseudonormal. *IEEE Transactions on Visualization and Computer Graphics* 11, 3 (2005), 243–253.

Gavin Barill, Neil G Dickson, Ryan Schmidt, David IW Levin, and Alec Jacobson. 2018. Fast winding numbers for soups and clouds. *ACM Transactions on Graphics (TOG)* 37, 4 (2018), 1–12.

Gianmarco Cherchi, Fabio Pellacini, Marco Attene, and Marco Livesu. 2022. Interactive and Robust Mesh Booleans. *ACM Trans. Graph.* 41, 6, Article 248 (nov 2022), 14 pages. https://doi.org/10.1145/3550454.3555460

Herbert Edelsbrunner and Ernst P Mücke. 1994. Three-dimensional alpha shapes. *ACM Transactions On Graphics (TOG)* 13, 1 (1994), 43–72.

Alec Jacobson, Ladislav Kavan, and Olga Sorkine-Hornung. 2013. Robust inside-outside segmentation using generalized winding numbers. *ACM Transactions on Graphics (TOG)* 32, 4 (2013), 1–12.

Charlie CL Wang and Dinesh Manocha. 2013. GPU-based offset surface computation using point samples. *Computer-Aided Design* 45, 2 (2013), 321–330.

Daniel Zint, Nissim Maruani, Mael Rouxel-Labbé, and Pierre Alliez. 2023. Feature-Preserving Offset Mesh Generation from Topology-Adapted Octrees. In *Computer Graphics Forum*. 12.

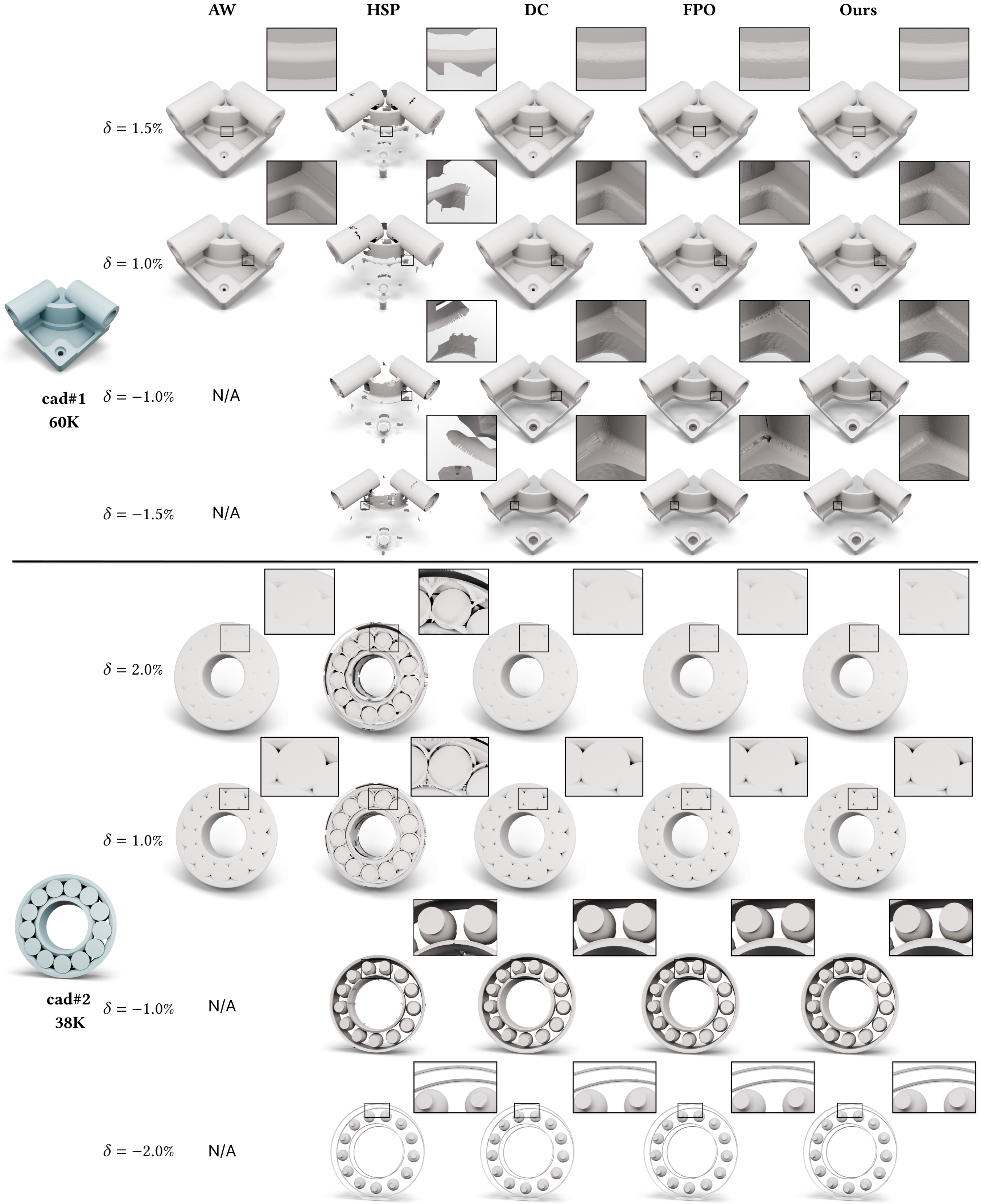

Fig. 4. Visual comparison results on cad models (part one).

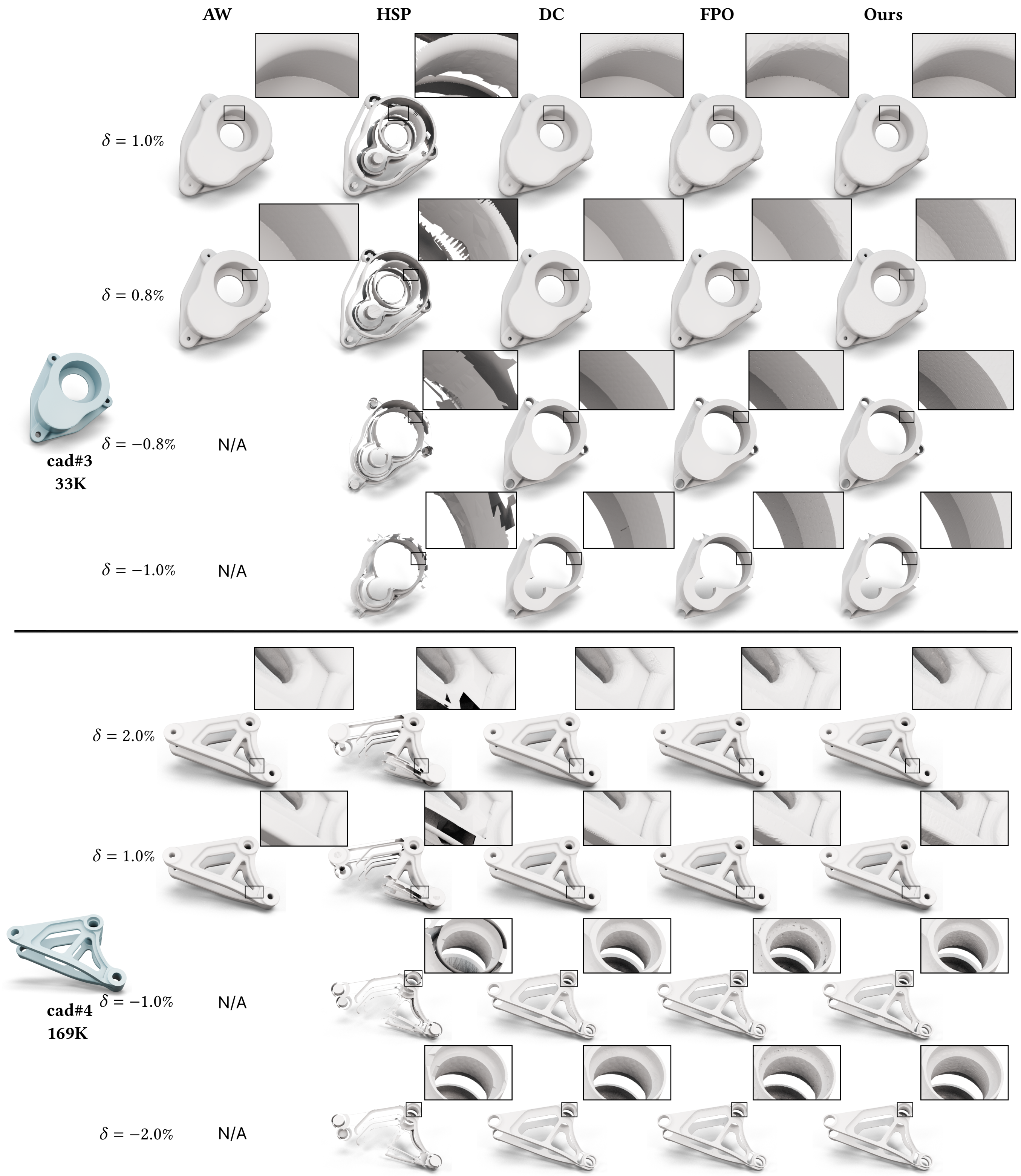

Fig. 5. Visual comparison results on cad models (part two).

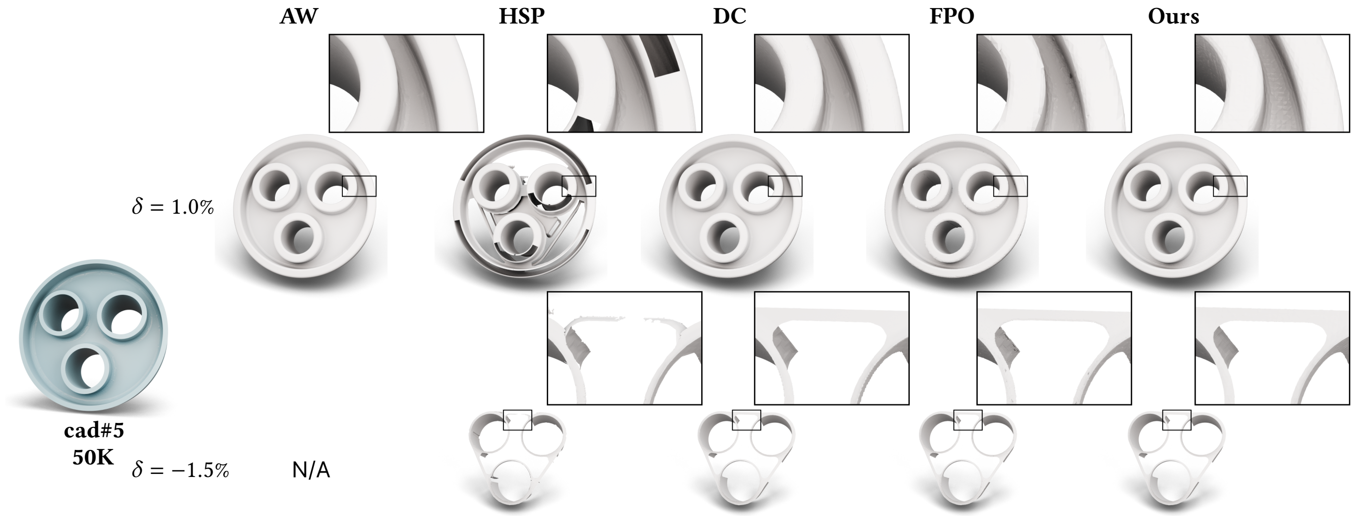

Fig. 6. Visual comparison results on cad models (part three).

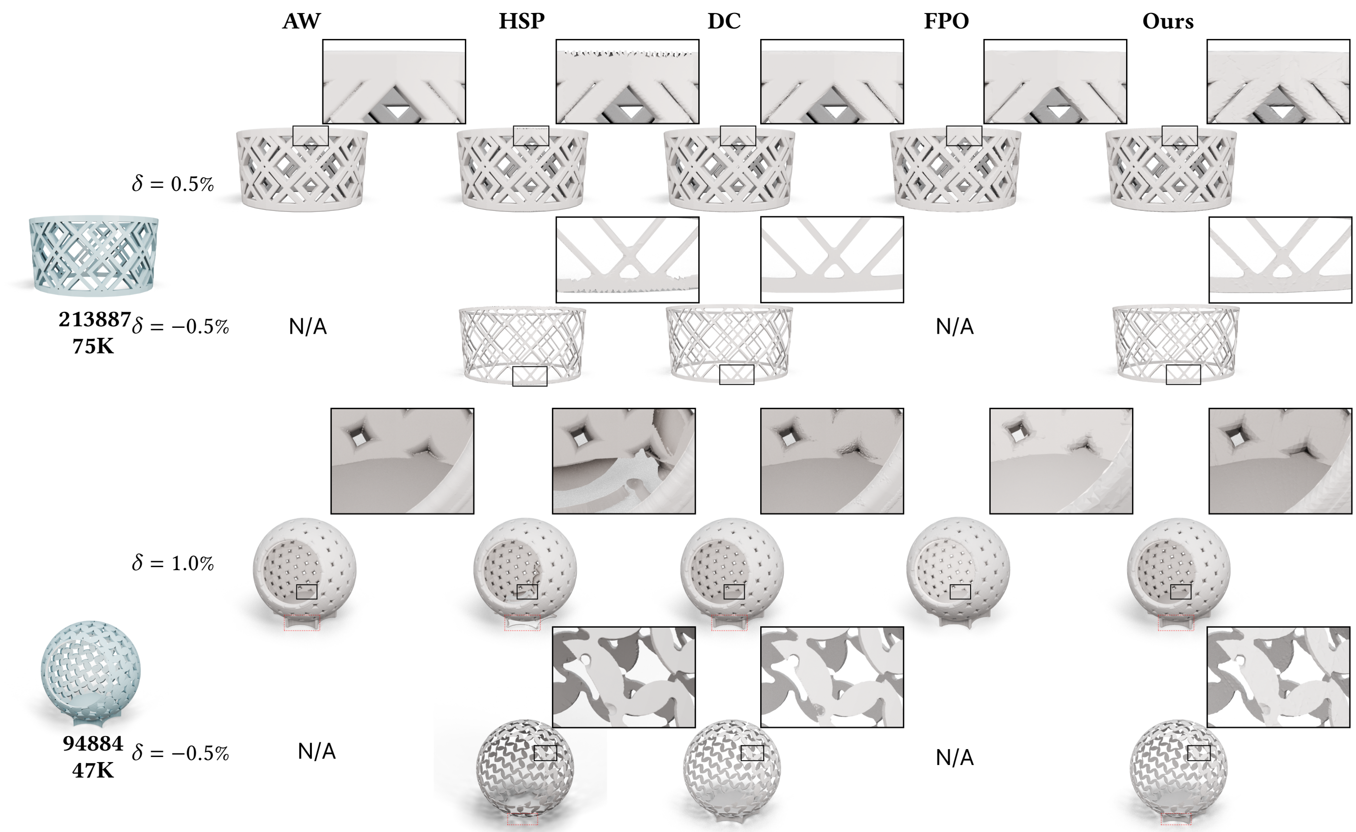

Fig. 7. Visual comparison results on twisted and thin-plate models.

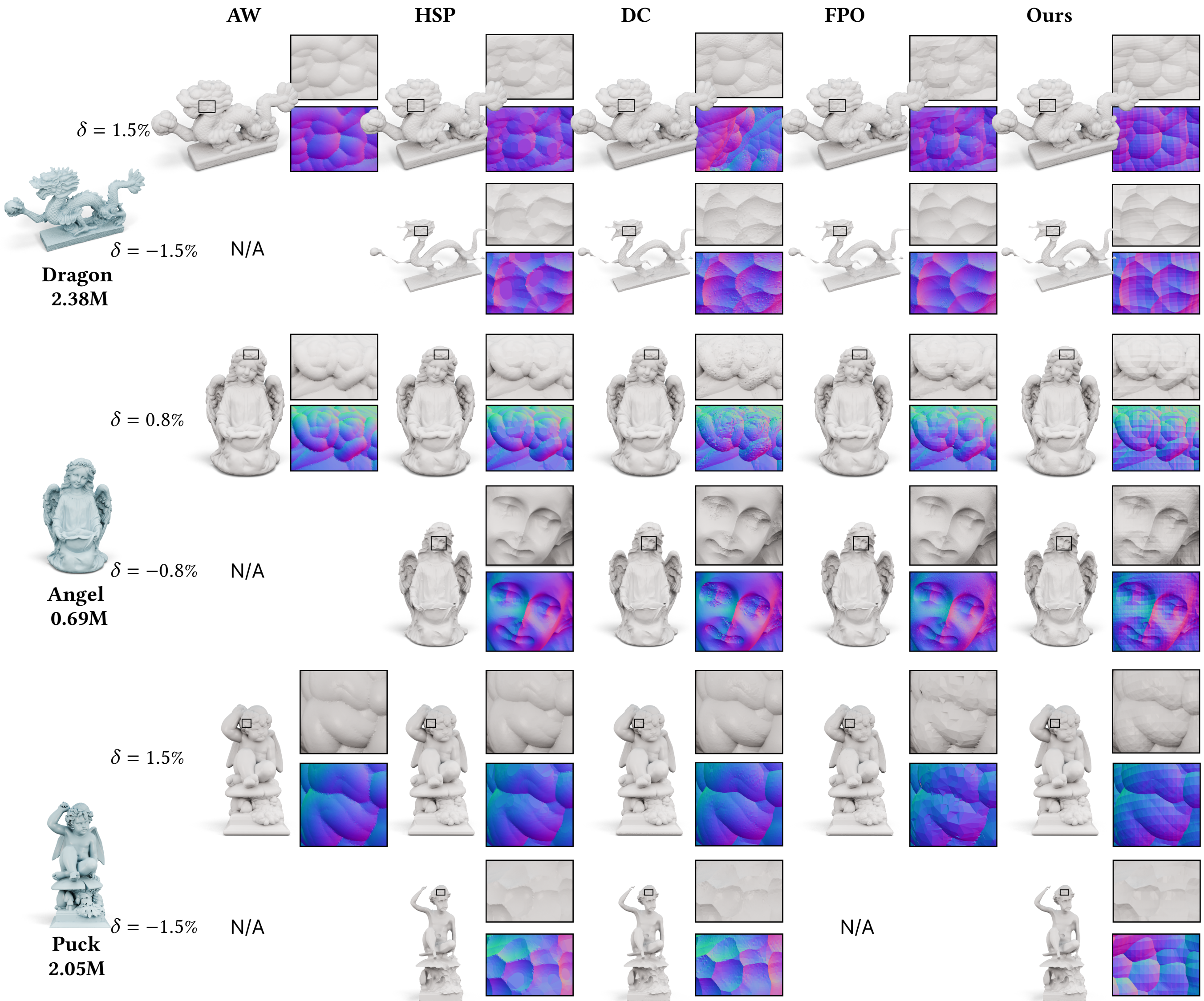

Fig. 8. Visual comparison results on models reconstructed from large raw scans.

Table 2. Quantitative comparison results on cad models. The **best** scores are highlighted in bold with underlining, while the **second best** scores are highlighted in bold.

		cad#1				cad#2				cad#3				cad#4				cad#5			
		-1.5	-1	1	1.5	-2	-1	1	2	-1	-0.8	0.8	1	-2	-1	1	2	-1.5	-1	1	1.5
Time/s	AW	-	-	224.57	228.49	-	-	128.24	131.17	-	-	68.627	100.17	-	-	170.18	101.60	-	-	157.53	185.2
	DC	252.46	269.65	275.78	258.20	110.37	106.81	112.87	109.23	99.62	95.07	101.89	97.23	166.25	205.66	210.34	170.02	109.04	182.96	187.11	111.52
	FPO	457.82	542.72	180.26	200.44	747.77	758.11	40.39	40.10	423.72	446.47	112.67	118.48	1020.00	1989.50	608.85	380.51	503.00	3067.40	72.39	76.29
	HSP	**20.40**	**16.12**	**23.51**	**30.83**	**5.16**	**4.47**	**8.73**	**11.15**	**3.19**	**2.76**	**8.15**	**8.49**	**44.35**	**25.66**	**30.15**	**45.41**	**11.90**	**10.59**	**19.37**	**23.91**
	Ours	**9.97**	**6.32**	**7.98**	**10.6**	**9.54**	**6.47**	**6.51**	**9.24**	**4.80**	**4.59**	**5.69**	**6.08**	**25.06**	**26.79**	**17.07**	**21.72**	**5.17**	**8.37**	**9.49**	**12.25**
d_C ($\times 10^{-3}$) ↓	AW	-	-	**0.431**	**0.312**	-	-	**0.595**	**0.296**	-	-	**1.007**	**0.801**	-	-	**1.639**	**0.187**	-	-	**0.539**	**0.313**
	DC	**0.678**	**0.887**	1.621	1.509	**0.683**	**0.732**	**1.248**	1.314	**0.570**	**0.613**	**1.972**	2.246	**1.062**	**0.336**	**1.057**	1.139	**0.729**	**4.959**	**1.270**	**0.824**
	FPO	**1.594**	2.878	3.659	3.891	0.951	3.420	3.994	5.168	**4.125**	4.704	4.547	6.201	1.476	2.553	3.398	3.558	**1.874**	**4.373**	5.272	5.170
	HSP	22.299	26.896	94.822	58.516	16.078	48.624	39.345	17.101	80.463	115.02	47.044	45.349	19.832	9.9452	40.625	37.470	2.904	5.330	18.051	10.861
	Ours	2.940	**0.798**	**0.990**	**0.768**	**0.161**	**2.261**	4.308	**1.156**	9.131	**3.079**	10.253	**1.220**	**0.343**	**0.628**	2.664	**0.315**	3.610	6.551	2.251	1.145
d_H ($\times 10^{-3}$) ↓	AW	-	-	**31.744**	**26.164**	-	-	**33.560**	**17.670**	-	-	**41.88**	**27.072**	-	-	70.888	**9.994**	-	-	**12.837**	**9.139**
	DC	**34.482**	**62.565**	88.972	56.223	**20.487**	**26.700**	45.367	44.463	**25.262**	**28.27**	51.296	37.618	**26.174**	**9.978**	**28.822**	17.644	**28.688**	**58.766**	38.301	27.256
	FPO	282.020	257.918	106.221	128.380	28.392	209.376	102.918	234.157	222.069	285.950	111.776	109.244	43.971	45.908	74.847	60.612	82.414	186.455	104.821	115.673
	HSP	963.813	1181.667	3963.144	2559.523	325.106	951.220	917.804	478.320	1778.204	3551.278	1909.256	1761.066	576.751	119.336	456.150	293.358	112.661	89.375	121.893	57.095
	Ours	**24.092**	**80.294**	**20.289**	**20.215**	**20.424**	**59.827**	**38.832**	**10.420**	**19.720**	**37.309**	**48.731**	**10.58**	**0.645**	**1.287**	**31.256**	**6.644**	**23.100**	**48.833**	**20.681**	**10.436**
N_{MAE} ↓	AW	-	-	**2.385**	**3.254**	-	-	3.388	5.234	-	-	**5.383**	**5.444**	-	-	5.863	7.585	-	-	**2.397**	**3.917**
	DC	**1.621**	**1.216**	**2.347**	3.418	**2.778**	**1.869**	**2.615**	**5.113**	**4.705**	**4.451**	6.736	7.451	**5.009**	**1.257**	**4.552**	**7.537**	**2.600**	**10.248**	**2.883**	4.367
	FPO	3.524	3.709	2.830	4.297	5.450	4.694	4.018	6.395	9.612	8.048	7.894	7.476	7.966	5.553	5.442	8.975	6.827	22.711	3.950	6.045
	HSP	74.015	66.633	58.282	43.466	105.75	86.414	30.973	28.216	95.559	38.914	8.440	11.420	48.301	58.266	55.195	65.005	169.910	99.670	3.430	5.432
	Ours	**1.468**	**3.061**	3.086	**2.182**	**1.446**	**3.391**	**3.378**	**1.737**	**3.625**	**4.738**	**4.540**	**3.582**	**2.464**	**4.931**	**5.075**	**2.514**	**2.206**	**3.398**	3.348	**2.257**
N-Score/% ↑	AW	-	-	**91.41**	**88.20**	-	-	**86.72**	76.08	-	-	**76.53**	**75.66**	-	-	**83.24**	76.42	-	-	**89.50**	83.08
	DC	**94.61**	**95.81**	**92.26**	87.79	**87.21**	**91.83**	**87.82**	**78.68**	**88.93**	**91.69**	**78.37**	75.21	**79.17**	**95.29**	**85.89**	**77.34**	**86.18**	**67.13**	**89.52**	**84.42**
	FPO	85.95	**87.33**	90.95	86.06	73.36	**80.00**	84.80	73.50	71.22	**72.65**	**72.45**	70.63	55.46	**66.42**	82.23	73.76	71.52	62.16	84.18	78.37
	HSP	48.24	57.55	60.70	67.38	23.22	40.79	65.65	57.14	28.54	54.13	66.15	64.26	55.32	57.83	39.07	23.60	2.41	36.71	84.52	77.81
	Ours	**94.67**	78.62	78.76	**90.93**	**97.46**	74.43	85.23	**94.21**	**83.70**	62.45	63.57	**82.17**	**89.06**	61.41	59.60	**90.22**	**88.93**	**74.79**	75.86	**89.25**

Table 3. Quantitative comparison results on models reconstructed from large raw scan data. The **best** scores are highlighted in bold with underlining, while the **second best** scores are highlighted in bold.

		Angel				Dragon				Puck			
		-1.5	-0.8	0.8	1.5	-2	-1.5	1.5	2	-2	-1.5	1.5	2
Time/s	AW	-	-	244.59	222.89	-	-	**146.89**	**159.88**	-	-	259.17	**187.23**
	DC	360.98	331.08	338.61	369.19	1203.00	1160.91	1187.33	1230.44	1064.32	1077.46	1101.97	1118.53
	FPO	8231.20	8160.30	1820.03	1678.08	7573.34	9054.40	5206.51	5350.55	-	-	8243.60	4422.47
	HSP	**26.88**	**16.25**	**21.96**	**36.65**	**9.35**	**8.50**	**15.41**	**17.54**	**27.03**	**22.62**	**28.93**	**35.63**
	Ours	**58.51**	**30.63**	**32.68**	**67.73**	**462.73**	**257.45**	391.37	620.47	**315.06**	**220.17**	**237.87**	327.32
d_C ($\times 10^{-3}$) ↓	AW	-	-	**1.786**	**3.008**	-	-	**1.423**	**1.098**	-	-	**1.006**	0.599
	DC	3.168	**3.853**	**3.293**	**2.641**	**2.228**	**2.467**	**2.594**	2.150	**0.837**	**1.195**	**0.676**	**0.593**
	FPO	**1.635**	**3.304**	5.439	6.954	**1.107**	**1.621**	12.754	12.742	-	-	6.787	8.290
	HSP	5.776	9.365	10.304	5.385	4.048	6.260	9.379	6.206	4.171	6.791	6.371	4.149
	Ours	**2.358**	7.414	6.665	8.815	2.883	4.990	3.590	**1.114**	**0.132**	**2.118**	3.956	**0.420**
d_H ($\times 10^{-3}$) ↓	AW	-	-	**54.409**	77.075	-	-	**27.258**	**22.782**	-	-	34.884	18.534
	DC	55.081	111.49	79.617	**66.593**	26.193	**29.415**	**26.082**	24.576	**22.468**	**33.091**	**19.44**	**13.772**
	FPO	**28.884**	**33.810**	60.953	321.060	**17.287**	**25.186**	651.770	350.560	-	-	138.239	284.792
	HSP	264.311	383.820	149.6	86.129	82.456	105.96	246.86	66.947	99.041	100.816	108.522	190.982
	Ours	**23.370**	**43.771**	**44.020**	**63.401**	**20.828**	32.739	29.981	**13.688**	**12.216**	**35.249**	**22.312**	**8.367**
N_{MAE} ↓	AW	-	-	**3.589**	4.393	-	-	**4.322**	**4.381**	-	-	4.153	4.048
	DC	7.767	**5.237**	4.674	6.239	22.977	19.020	7.219	7.431	**6.112**	**6.544**	**2.594**	**3.486**
	FPO	8.982	8.092	5.316	7.095	18.799	18.322	8.018	8.581	-	-	64.623	58.696
	HSP	**5.670**	**4.119**	**4.225**	**3.997**	18.871	16.708	**4.953**	4.541	8.296	6.764	**3.485**	**3.509**
	Ours	**3.495**	6.729	6.309	**3.304**	**4.153**	**5.541**	6.014	**3.902**	**3.465**	**4.705**	4.639	3.703
N-Score/% ↑	AW	-	-	**80.70**	73.50	-	-	**76.80**	**77.63**	-	-	80.50	78.66
	DC	65.10	**74.83**	**79.07**	71.33	5.55	56.53	62.64	62.00	**67.71**	**71.28**	**86.80**	**83.93**
	FPO	51.46	55.80	70.22	57.91	62.20	61.50	46.23	43.31	-	-	43.51	38.93
	HSP	**71.10**	**77.68**	75.40	**74.62**	**65.73**	**67.00**	**69.63**	**72.46**	59.26	67.05	**82.51**	80.13
	Ours	**75.84**	60.55	62.76	**80.00**	**69.16**	**61.67**	65.54	70.65	**80.07**	**78.67**	80.70	**84.91**